Jagannath University Journal of Science
Volume 12, Number II, Dec. 2025, pp. 119−142
https://jnu.ac.bd/journal/portal/archives/science.jsp
ISSN 3005-4486 (Online), ISSN 2224-1698 (Print)

Optimal Control and Cost-Effective Management of COVID-19 Epidemic Model Using a Vaccination SEIAVR Framework with Bang–Bang Control

Research Article

Md. Habibur Rahman, Mostak Ahmed*, Md. Abdullah Bin Masud

Department of Mathematics, Jagannath University, Dhaka-1100, Bangladesh

DOI: https://doi.org/10.3329/jnujsci.v12i2.89625

Received: 18.12.2025, Accepted: 02.03.2026, Published: July 2026

ABSTRACT

The global spread of COVID-19 highlighted the necessity of control strategies that are not only epidemiologically effective but also economically viable. Designing such interventions requires balancing transmission reduction with associated implementation costs. Many existing mathematical models rely on continuous control mechanisms and do not explicitly connect cost-effectiveness analysis with observed epidemiological data. In this work, we first formulate a SEIAR compartmental model and subsequently extend it to a vaccination-incorporated SEIAVR framework. To capture the realistic implementation of sudden public health measures, we employ a Bang–Bang optimal control approach. The basic reproduction number is derived and the local stability of the equilibria is rigorously analyzed. The optimal control structure is characterized using the Pontryagin Maximum Principle. Model validation and policy assessment are carried out through numerical simulations calibrated with COVID-19 data from the United Kingdom. The findings indicate that the integration of vaccination with Bang–Bang interventions significantly suppresses infection peaks and reduces the duration of the overall outbreak. From an economic perspective, the combined strategy achieves improved cost-effectiveness compared to non-vaccination scenarios. Although the model assumes homogeneous mixing and simplifies certain operational aspects of intervention deployment, it offers a mathematically grounded and practically relevant framework for rapid-response policy design, contributing to the integration of epidemiological dynamics and economic optimization in infectious disease modeling.

Keywords: *Optimal Control, Bang-Bang Control, Cost-Effectiveness, Stability Analysis, Hamiltonian Equation, Pontryagin's Maximum Principle*

1. Introduction

The global spread of infectious diseases continues to pose severe challenges to public health systems, social stability, and economic sustainability [1]. The COVID-19 pandemic, caused by the SARS-CoV-2 virus, has become one of the most destructive public

* **Corresponding author:** Mostak Ahmed
E-mail: mostak@math.jnu.ac.bd

health crises in modern history due to its rapid spread, the presence of asymptomatic carriers, delays in testing and diagnosis, and the continuous emergence of viral variants [2, 3, 4]. Since its emergence in late 2019, COVID-19 has caused unprecedented morbidity, mortality, and severe economic losses worldwide [5]. Despite large-scale implementation of pharmaceutical and non-pharmaceutical interventions, including vaccination, lockdowns, and mass testing and treatment programs, many countries continue to face challenges in balancing effective disease control with limited medical resources and economic constraints [6, 7]. These challenges highlight the necessity of establishing a mathematically grounded framework capable of evaluating intervention strategies not only in terms of epidemiological effectiveness but also from an economic feasibility perspective [8]. In this context, mathematical epidemiological models incorporating optimal control theory provide a powerful tool for understanding disease transmission dynamics and for designing timely, cost-effective intervention policies under real-world resource constraints [9, 10]. In practice, such mathematical models serve as essential decision-support tools for public health authorities by enabling policymakers to predict outbreak scenarios, compare intervention strategies, and make informed decisions under uncertainty.

To study the dynamic evolution of COVID-19, various compartmental epidemiological models have been proposed, including SEIAR frameworks that incorporate susceptible individuals , exposed individuals, asymptomatic carriers, infected populations, and recovery compartments [3, 11]. Many studies employ optimal control theory to assess intervention strategies such as vaccination, isolation, treatment, social distancing, and public awareness campaigns [8]. Continuous optimal control approaches based on the Pontryagin maximum principle have been widely used to minimize infection prevalence while reducing intervention related costs [9]. Meanwhile, cost-effectiveness analysis (CEA) has become an important tool for comparing alternative control strategies using indicators such as the average cost-effectiveness ratio (ACER) and the incremental cost-effectiveness ratio (ICER) [12]. These methods enhance decision-making by explicitly quantifying trade-offs between health outcomes and economic costs. However, most existing studies assume smooth and continuous variations in control intensity, which may not adequately capture the abrupt and frequent policy shifts observed in real-world public health responses [13]. Over the past several years, substantial attention has been given to vaccination-based control strategies, early case detection, and treatment optimization in the context of COVID-19 and related infectious diseases [11, 14, 8]. These studies have clarified the importance of intervention timing and coverage levels in shaping outbreak trajectories. Nevertheless, certain modeling aspects remain insufficiently explored. In particular, the distinction between mild or asymptomatic infections and severe cases is often overlooked when estimating treatment demand and the associated economic burden. This simplification may lead to an incomplete assessment of healthcare resource allocation.

Another practical concern is the widespread reliance on continuously varying control functions. Although mathematically convenient, such strategies do not always reflect the way public health measures are implemented in reality. Governments frequently introduce or withdraw interventions abruptly for example, through emergency lockdowns, rapid treatment expansion, or sudden policy relaxation. Furthermore, cost-effectiveness considerations are commonly appended to epidemiological analyses rather than embedded directly within the control framework. Only a limited number of studies attempt to evaluate economic outcomes alongside epidemiological predictions using calibrated real-world data [12, 13].

Motivated by these observations, we develop a vaccination-enhanced SEIAVR model that incorporates an optimal Bang–Bang control formulation. The analytical foundation is provided

by the Pontryagin Maximum Principle, which enables the derivation of necessary optimality conditions under bounded intervention policies. This framework is particularly appropriate for modeling abrupt control actions and yields strategies with clear epidemiological interpretation. In addition to theoretical analysis such as the derivation of threshold conditions and stability results numerical simulations are conducted to examine the temporal dynamics of the system. Model parameters are calibrated using COVID-19 data from the United Kingdom to ensure practical relevance. By integrating treatment-oriented control, vaccination dynamics, and cost-effectiveness indicators such as ACER and ICER within a unified framework, the study aims to provide a more policy-aligned assessment of intervention strategies. The results are intended to support evidence-based decision-making by linking epidemic control performance with economic evaluation in a transparent and mathematically consistent manner.

2. Preliminaries and Model Formulation

2.1 Preliminaries

Definition 1 *Consider a control function* $u(t)$ *constrained by*

$$u_{\min} \le u(t) \le u_{\max}, \quad \forall t \in [0, T],$$

where $u_{\min}$ and $u_{\max}$ denote the minimum and maximum allowable control efforts [15], respectively. A Bang-Bang control implies that the optimal solution $u^*(t)$ satisfies

$$u^*(t) = \begin{cases} u_{\min}, & \text{if} \Phi(t) > 0, \\ u_{\max}, & \text{if} \Phi(t) < 0, \end{cases}$$

where $\Phi(t)$ is the switching function derived from Pontryagin's Maximum Principle (PMP).

Definition 2 *Cost-effectiveness analysis (CEA) is a method used to compare the costs and health outcomes of different intervention strategies. It helps determine which option provides the best outcome for the least cost. Two key metrics in CEA are the Average Cost-Effectiveness Ratio (ACER) [16],*

$$ACER = \frac{\text{TotalCost}}{\text{TotalInfectionsAverted}},$$

and the Incremental Cost-Effectiveness Ratio (ICER),

$$ICER = \frac{C_2 - C_1}{E_2 - E_1},$$

where C_i and E_i represent the cost and effectiveness of strategy i. A strategy is more cost-effective if it achieves better outcomes at a lower or reasonable cost.

2.2 Model Formulation: Construction of the model without vaccination

We begin by constructing a compartmental SEIAR model to represent the transmission dynamics of COVID-19, as shown in Fig. 1. The total population at any time t, denoted by $N(t)$, is divided into five compartments. $S(t)$ denotes the susceptible individuals who are healthy and at risk of infection, $E(t)$ represents the exposed individuals who are infected but not yet infectious, $I(t)$ refers to symptomatic infectious individuals who can transmit the virus and exhibit symptoms, $A(t)$ indicates asymptomatic infectious individuals who can transmit the virus without showing symptoms and $R(t)$ includes those who have recovered and acquired temporary immunity.

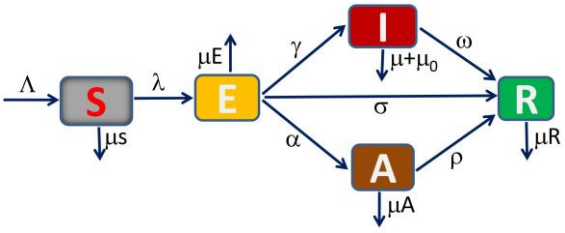

Figure 1: Flowchart of the COVID-19 transmission model without vaccination

The dynamics of the system illustrated in Fig. 1 are described by the following set of nonlinear differential equations

$$\begin{cases} \frac{dS}{dt} = \Lambda - \beta \frac{S}{N}(I + k_1 E + k_2 A) - \mu S, \\ \frac{dE}{dt} = \beta \frac{S}{N}(I + k_1 E + k_2 A) - (\mu + \gamma + \sigma + \alpha)E, \\ \frac{dI}{dt} = \gamma E - (\mu + \mu_0 + \omega)I, \\ \frac{dA}{dt} = \alpha E - (\rho + \mu)A, \\ \frac{dR}{dt} = \omega I + \sigma E + \rho A - \mu R. \end{cases} \quad (1)$$

The model (1) starts with the following non-negative initial conditions

$$S(0) \geq 0, \quad E(0) \geq 0, \quad I(0) \geq 0, \quad A(\geq 0,$$

$$R(0) \geq 0.$$

In Eq. (1), the total population is divided into five epidemiological compartments, each representing a different stage of COVID-19 transmission. The susceptible population S consists of individuals at risk of infection. Individuals enter this population at a rate λ through recruitment and exit at a rate μ through natural death.

The exposed population E represents individuals who are infected but have not yet developed full symptoms. These individuals may still transmit the virus at a lower level. The infection process is controlled by the following formula:

$$\beta \frac{S}{N}(I + k_1 E + k_2 A),$$

where β is the effective transmission rate, and k_1 and k_2 are correction factors used to explain the relative infectivity of the exposed population and asymptomatic individuals. This model reflects epidemiological evidence that asymptomatic and pre-symptomatic individuals can also promote the spread of COVID-19.

After the incubation period, exposed individuals may develop symptomatic infections (Category I) at a rate of γ, asymptomatic infections (Category A) at a rate of α, or recover directly without showing obvious symptoms at a rate of σ. The parameter σ represents individuals who clear the infection during the incubation period, i.e., mild or undetected cases.

Symptomatic individuals recover at a rate of ω or die from the disease at a rate of μ_0, while asymptomatic individuals recover at a rate of ρ. A recovered individual is defined as an individual who has acquired immunity after infection.

This baseline SEIAR model provides a structured description of the transmission dynamics of COVID-19, highlighting in particular the role of asymptomatic and latent infections. In the next section, the model will be extended to incorporate vaccination and "one-hit-kill" control strategies to assess their epidemiological and economic impacts. For ease of further analysis, model parameters, baseline values, and corresponding data sources are summarized in Table 1.

2.3 Stability of the Disease-Free Equilibrium

We now analyze the qualitative dynamics of the system of Eq. (1), focusing on the disease-free equilibrium (DFE). The feasible region for the system is defined by

$$\Omega = \left\{(S, E, A, I, R) \in \mathbb{R}_+^5 | S + E + A + I + R \leq \frac{\Lambda}{\mu}\right\}. \quad (2)$$

The region Ω is positively invariant and attracting, ensuring that any trajectory starting in Ω remains in Ω for all $t > 0$. Therefore, the model is both mathematically and biologically well-posed within this domain.

To examine the local stability of the DFE, we set the right-hand sides of system of Eq. (1) to zero. The unique disease-free equilibrium is:

$$E_0 = (S^0, E^0, A^0, I^0, R^0) = \left(\frac{\Lambda}{\mu}, 0,0,0,0\right).$$

We apply the next-generation matrix method [22] to determine the basic reproduction number $\mathcal{R}_0$. The infectious compartments are E, I, A. Let $\mathbf{x} = (E, I, A)^\top$. The vector of new infections $\mathcal{F}(\mathbf{x})$ and the transition terms $\mathcal{V}(\mathbf{x})$ are given by:

$$\mathcal{F} = \begin{pmatrix} \beta \frac{S^0}{N}(I + k_1 E + k_2 A) \\ 0 \\ 0 \end{pmatrix},$$

$$\mathcal{V} = \begin{pmatrix} (\mu + \gamma + \sigma + \alpha)E \\ -\gamma E + (\mu + \mu_0 + \omega)I \\ -\alpha E + (\rho + \mu)A \end{pmatrix}.$$

Linearizing $\mathcal{F}$ and $\mathcal{V}$ at the DFE E_0, we obtain the matrices F and V:

$$F = \begin{pmatrix} \beta k_1 & \beta & \beta k_2 \\ 0 & 0 & 0 \\ 0 & 0 & 0 \end{pmatrix},$$

$$V = \begin{pmatrix} \mu+\gamma+\sigma+\alpha & 0 & 0 \\ -\gamma & \mu+\mu_0+\omega & 0 \\ -\alpha & 0 & \rho+\mu \end{pmatrix}.$$

Then, the next-generation matrix is FV^{-1}, and the basic reproduction number $\mathcal{R}_0$ is the spectral radius $\rho(FV^{-1})$. Direct computation yields:

$$\mathcal{R}_0 = \frac{\beta}{\mu+\gamma+\sigma+\alpha}\left(\frac{\gamma}{\mu+\mu_0+\omega} + k_1 + \frac{\alpha k_2}{\rho+\mu}\right). \quad (3)$$

This expression represents the combined contributions to new infections from three pathways: Direct exposure infectiousness k_1, Secondary infections from symptomatic individuals $I(t)$, Infections caused by asymptomatic individuals $A(t)$.

The disease-free equilibrium E_0 is locally asymptotically stable if $\mathcal{R}_0 < 1$ and unstable if $\mathcal{R}_0 > 1$.

2.4 The Vaccination-Enhanced COVID-19 Model (SEIAVR)

Table 1: The parameters are outlined in the table below.

Notation	Description	Values	Refs.
$S(0)$	Initial number of susceptible individuals	10 Crore	Proposed
$E(0)$	Initial number of exposed individuals	05 Crore	Proposed
$I(0)$	Initial number of infectious individuals	05 lacs	Proposed
$A(0)$	Initial number of asymptomatic individuals	02 lacs	Proposed
$R(0)$	Initial number of recovered individuals	0	Proposed
Λ	Recruitment/immigration rate (per day)	0.004371	[17]
μ	Natural death rate (per day)	$1/(74.87 * 365)$	[17]
μ_0	Disease-induced death rate (per day)	0.02320	[18]
β	Effective contact rate (per day)	0.26000	[19]
k_1	Infectiousness factor of exposed individuals	0.51310	[20]
k_2	Infectiousness factor of asymptomatic individuals	0.42113	[20, 21]
λ	Exposure rate (per day)	0.04545	[20]
γ	Progression rate from E to I (per day)	0.00437	[18]
σ	Recovery rate from E (per day)	0.00122	[18]
α	Transition rate from E to A (per day)	0.00900	[19]
ω	Recovery rate from I (per day)	0.52000	[19]
ρ	Recovery rate from A to R (per day)	0.00850	[19]

The SEIAR framework, as discussed In Eq.(1), provides a foundation for studying COVID-19 transmission in the absence of vaccination. However, vaccination has proven to be one of the most effective measures in reducing infection rates and mitigating severe outcomes. To incorporate this intervention, we extend the baseline model by introducing a vaccinated class, resulting in the

SEIAVR formulation. This modification enables a more realistic assessment of epidemic control and the evaluation of vaccination strategies in combination with optimal control measures.

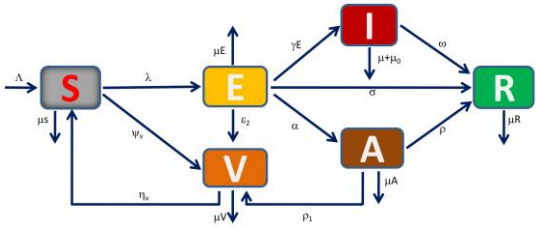

Figure 2: Schematic diagram of the COVID-19 transmission model incorporating vaccination.

Fig. 3 shows the schematic diagram of the extended COVID-19 model that incorporates vaccination. Where $S(t), E(t), I(t), A(t)$ and $R(t)$ has the same meaning as Eq. (1) and $V(t)$ stands for vaccinated individuals with partial or waning immunity. The total population is given by

$$N(t) = S(t) + E(t) + I(t) + A(t) + V(t) + R(t). \quad (4)$$

Both vaccinated individuals $V(t)$ and recovered individuals $R(t)$ may lose immunity over time and return to the susceptible class $S(t)$. Transmission occurs through contact between susceptible individuals and infectious individuals from the $E(t)$, $I(t)$, and $A(t)$ compartments. The modification parameters k_1 and k_2 represent the relative infectiousness of the exposed and asymptomatic classes, respectively. The force of infection is defined by

$$\lambda_1(t) = \beta \frac{I(t)+k_1E(t)+k_2A(t)}{N(t)}, \quad (5)$$

where β denotes the effective contact rate. The SEIAVR model is governed by the following system of nonlinear differential equations

$$\begin{cases} \frac{dS(t)}{dt} = \Lambda - \beta(I(t) + k_1E(t) + k_2A(t))\frac{S(t)}{N(t)} + \eta_v V(t) + \theta R(t) - (\phi_v + \mu)S(t), \\ \frac{dE(t)}{dt} = \beta(I(t) + k_1E(t) + k_2A(t))\frac{S(t)}{N(t)} - (\mu + \gamma + \epsilon_2 + \sigma + \alpha)E(t), \\ \frac{dI(t)}{dt} = \gamma E(t) - (\mu + \mu_0 + \omega)I(t), \\ \frac{dA(t)}{dt} = \alpha E(t) - (\rho + \rho_1 + \mu)A(t), \\ \frac{dV(t)}{dt} = \phi_v S(t) + \epsilon_2 E(t) + \rho_1 A(t) - (\mu + \eta_v)V(t), \\ \frac{dR(t)}{dt} = \omega I(t) + \sigma E(t) + \rho A(t) - (\mu + \theta)R(t). \end{cases} \quad (6)$$

The Eq. (6) starts with the following non-negative initial conditions $S(0) \geq 0$, $E(0) \geq 0$, $I(0) \geq 0$, $A(0) \geq 0$, $V(0) \geq 0$, $R(0) \geq 0$.

Table 2: Model parameters with their descriptions, values, and references.

Notation	Description	Values	Refs.
$V(0)$	Initial number of Vaccinated individuals	0	Proposed
λ	Exposure rate (per day)	0.04545	[23]
ϕ_v	Vaccination rate (per day)	0.08000	[20]
ϵ_2	Progression rate from E to V (per day)	0.00200	[24]
ρ_1	Transition rate from A to V (per day)	0.02763	[25]
η_v	Waning rate of vaccine-induced immunity	0.01957	[26]

For simplification, we rewrite the system using the force of infection $\lambda_1(t)$ from Eq. (6)

$$\begin{cases} \frac{dS(t)}{dt} = \Lambda - \lambda_1(t)S(t) + \eta_v V(t) + \theta R(t) - (\phi_v + \mu)S(t), \\ \frac{dE(t)}{dt} = \lambda_1(t)S(t) - (\mu + \gamma + \epsilon_2 + \sigma + \alpha)E(t), \\ \frac{dI(t)}{dt} = \gamma E(t) - (\mu + \mu_0 + \omega)I(t), \\ \frac{dA(t)}{dt} = \alpha E(t) - (\rho + \rho_1 + \mu)A(t), \\ \frac{dV(t)}{dt} = \phi_v S(t) + \epsilon_2 E(t) + \rho_1 A(t) - (\mu + \eta_v)V(t), \\ \frac{dR(t)}{dt} = \omega I(t) + \sigma E(t) + \rho A(t) - (\mu + \theta)R(t). \end{cases} \quad (7)$$

We simulate the SEIAVR shown in Eq. (7) to actively capture the dynamic interactions among all compartments. The graphical presentation plays a vital role here, as it visually demonstrates the temporal changes in susceptible, exposed, infected, asymptomatic, vaccinated, and recovered populations. Such visual representation not only makes the scenario more transparent but also enhances the understanding of the overall disease progression and the relative impact on each compartment.

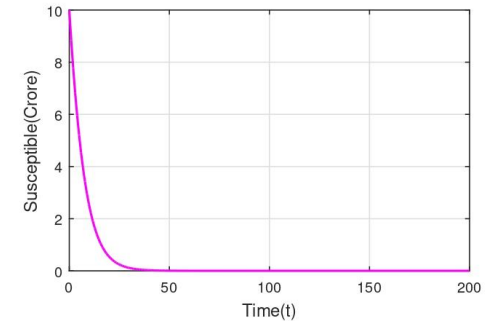

(a) Susceptible

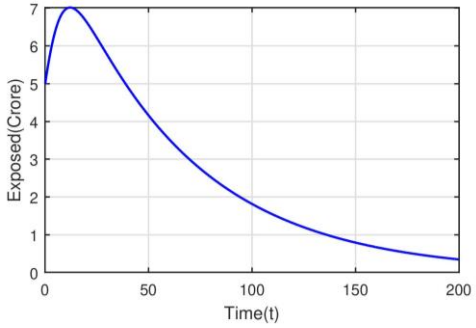

(b) Exposed

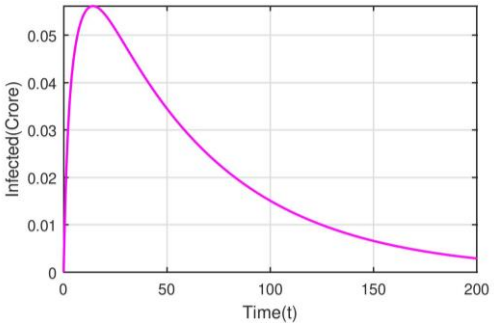

(c) Infected

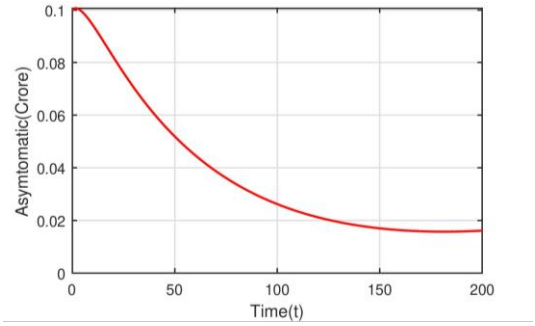

(d) Asymptomatic

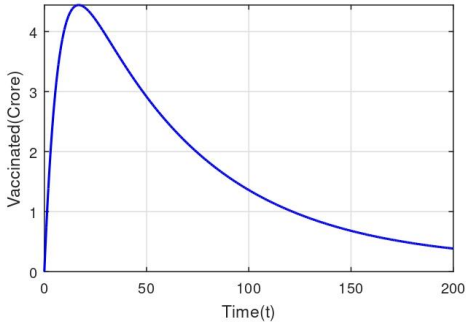

(e) Vaccinated

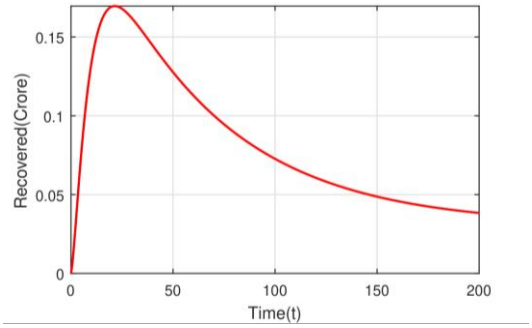

(f) Recovered

Figure 3: Scenario of state variables without control.

In the absence of any control interventions, the SEIAVR model simulation shown in Fig. 3 demonstrates a rapid and severe epidemic wave within the first month. The susceptible population, initially close to 10 crore, decreases rapidly and is nearly depleted by approximately day 25, suggesting an intense early transmission phase in which individuals transition quickly to either infection or vaccination. The exposed class increases sharply from zero and reaches a peak of nearly 6.8 crore around day 18. Thereafter, it steadily declines and becomes negligible before day 200.

In comparison, the symptomatic infectious population remains relatively small throughout the simulation, attaining a maximum of about 0.055 crore between days 20 and 25. The asymptomatic class exhibits a slightly higher peak, approximately 0.09 crore during a similar time interval, indicating the greater relative contribution of asymptomatic transmission. The vaccinated population rises to nearly 4.2 crore around day 28, reflecting the rapid implementation of immunization strategies. However, this level is not sustained; the vaccinated class gradually decreases to about 0.5 crore by the end of the simulation, primarily due to natural mortality and waning immunity.

The recovered population displays a delayed response compared to the infectious classes. It increases gradually and reaches a maximum of approximately 0.15 crore around day 38, after which it declines slowly to about 0.08 crore by day 200. Overall, the dynamics illustrate a sharp initial outbreak followed by progressive stabilization of all epidemiological compartments. Overall, the results indicate that without control measures, the infection spreads explosively, rapidly depletes the susceptible pool, and leaves only a small fraction of the population vaccinated or recovered by the end of the 200 days.

3. Stability Analysis of the DFE

To examine the local stability of the DFE, we employ the next-generation matrix method, a widely used framework for deriving the basic reproduction number $\mathcal{R}_v^0$. This threshold parameter quantifies the expected number of secondary infections produced by a single infectious individual in a fully susceptible population. In the SEIAVR model 6, the primary transmission dynamics involve the compartments $E(t)$, $I(t)$, $A(t)$, and $V(t)$. The force of infection contributing to the exposed class $E(t)$ is modeled as

$$\beta(I(t) + k_1E(t) + k_2A(t))\frac{S(t)}{N(t)}. \quad (8)$$

Although $V(t)$ represents the vaccinated population, it is included in the infected subsystem to capture the effects of waning immunity and delayed vaccine efficacy, which may influence transmission. The vector of new infection terms is then given by

$$f = \left[\beta(I(t) + k_1E(t) + k_2A(t))\frac{S(t)}{N(t)},\ 0,\ 0,\ 0\right]. \quad (9)$$

The vector V, representing transitions among infected compartments other than new infections, is formulated as

$$V = \begin{bmatrix}(\mu + \gamma + \epsilon_2 + \sigma + \alpha)E(t)\\ -\gamma E(t) + yI(t)\\ -\alpha E(t) + (\rho + \rho_1 + \mu)A(t)\\ -\phi_v S(t) - \epsilon_2 E(t) + \rho_1 A(t) - (\mu + \eta_v)V(t)\end{bmatrix}, \quad (10)$$

where $y = \mu + \mu_0 + \omega$ denotes the total removal rate of symptomatic individuals.

Let the infected state vector be $[E, I, A, V]$. Evaluating the Jacobian matrices of f and V at the DFE, we obtain

$$F = \begin{pmatrix}\beta k_1\frac{S_0}{N_0} & \beta\frac{S_0}{N_0} & \beta k_2\frac{S_0}{N_0} & 0\\ 0 & 0 & 0 & 0\\ 0 & 0 & 0 & 0\\ 0 & 0 & 0 & 0\end{pmatrix}. \quad (11)$$

At equilibrium, the susceptible population is given by $S_0 = \frac{\Lambda x}{\mu(x+\phi_v)}$, where $x = \mu + \eta_v$. Substituting this into F, we have

$$F = \beta\frac{\Lambda x}{N_0\mu(x+\phi_v)}\begin{pmatrix}k_1 & 1 & k_2 & 0\\ 0 & 0 & 0 & 0\\ 0 & 0 & 0 & 0\\ 0 & 0 & 0 & 0\end{pmatrix}. \quad (12)$$

The total equilibrium population is

$$N_0 = S_0 + V_0 = \frac{\Lambda x}{\mu(x+\phi_v)} + \frac{\Lambda\phi_v}{\mu(x+\phi_v)} = \frac{\Lambda}{\mu}.$$

The Jacobian matrix of V, evaluated at the DFE, is

$$V = \begin{pmatrix} \mu+\gamma+\epsilon_2+\sigma+\alpha & 0 & 0 & 0 \\ -\gamma & y & 0 & 0 \\ -\alpha & 0 & \rho+\rho_1+\mu & 0 \\ -\epsilon_2 & 0 & -\rho_1 & x \end{pmatrix}.$$

The inverse of V is given by

$$V^{-1} = \begin{pmatrix} \frac{1}{\mu+\gamma+\epsilon_2+\sigma+\alpha} & 0 & 0 & 0 \\ \frac{\gamma}{(\mu+\gamma+\epsilon_2+\sigma+\alpha)y} & \frac{1}{y} & 0 & 0 \\ \frac{\alpha}{(\mu+\gamma+\epsilon_2+\sigma+\alpha)(\rho+\rho_1+\mu)} & 0 & \frac{1}{\rho+\rho_1+\mu} & 0 \\ \frac{\epsilon_2}{(\mu+\gamma+\epsilon_2+\sigma+\alpha)(\rho+\rho_1+\mu)x} & 0 & \frac{\rho_1}{x(\rho+\rho_1+\mu)} & \frac{1}{x} \end{pmatrix}.$$

Multiplying F and V^{-1}, the next-generation matrix becomes

$$FV^{-1} = \begin{pmatrix} \frac{\beta x(k_1 y+\gamma+\alpha k_2)}{(\mu+\gamma+\epsilon_2+\sigma+\alpha)(x+\phi_v)y} & \frac{\beta x}{y(x+\phi_v)} & \frac{\beta k_2 x}{(x+\phi_v)(\rho+\rho_1+\mu)} & 0 \\ 0 & 0 & 0 & 0 \\ 0 & 0 & 0 & 0 \\ 0 & 0 & 0 & 0 \end{pmatrix}. \quad (13)$$

The basic reproduction number $\mathcal{R}_v^0$ is the spectral radius of FV^{-1}

$$\mathcal{R}_v^0 = \rho(FV^{-1}) = \frac{\beta x}{(\mu+\gamma+\epsilon_2+\sigma+\alpha)(x+\phi_v)}\left(k_1 + \frac{\gamma}{y} + \frac{\alpha k_2}{y}\right)$$
$$= \frac{\beta x(k_1 y+\gamma+\alpha k_2)}{(\mu+\gamma+\epsilon_2+\sigma+\alpha)(x+\phi_v)y}$$
$$= R_v^1 + R_v^2 + R_v^3.$$

Each term in $\mathcal{R}_v^0$ captures the contribution of a specific transmission pathway

$$R_v^1 = \frac{\beta\gamma x}{(\mu+\gamma+\epsilon_2+\sigma+\alpha)(x+\phi_v)y},$$

$$R_v^2 = \frac{\beta k_1 x}{(\mu+\gamma+\epsilon_2+\sigma+\alpha)(x+\phi_v)},$$

$$R_v^3 = \frac{\beta\alpha k_2 x}{(\mu+\gamma+\epsilon_2+\sigma+\alpha)(x+\phi_v)y}.$$

Here, R_v^1 quantifies the contribution from symptomatic individuals via progression from the exposed class, R_v^2 reflects direct transmission from the exposed class, and R_v^3 represents infections arising from asymptomatic individuals through the exposed compartment.

Theorem 1. *The DFE E_0 of the COVID-19 model represented by Eq. (1) is locally asymptotically stable if the basic reproduction number satisfies $\mathcal{R}_0 < 1$.*

Proof. To investigate the local stability of the DFE $E_0 = \left(\frac{\Lambda}{\mu}, 0,0,0,0\right)$, we linearize the system (1) around this equilibrium and compute the Jacobian matrix $J(E_0)$, which is given by

$$J(E_0) = \begin{pmatrix} -\mu & -\beta k_1 & -\beta & -\beta k_2 & 0 \\ 0 & \beta k_1 - \eta & \beta & \beta k_2 & 0 \\ 0 & \gamma & -(\mu+\mu_0+\omega) & 0 & 0 \\ 0 & \alpha & 0 & -(\rho+\mu) & 0 \\ 0 & \sigma & \omega & \rho & -\mu \end{pmatrix}, \quad (15)$$

where $\eta = \mu + \gamma + \sigma + \alpha$.

It is evident that two eigenvalues of $J(E_0)$ are $-\mu$, which are clearly negative. The remaining three eigenvalues are determined from the submatrix associated with the infectious compartments (E, I, A), yielding a characteristic polynomial of the form

$$\lambda^3 + \pi_1\lambda^2 + \pi_2\lambda + \pi_3 = 0,$$

where the coefficients are given by

$$\pi_1 = \mathrm{x} + \eta + (\rho + \mu),$$
$$\pi_2 = \mathrm{x}(\eta + \rho + \mu) + (\rho + \mu)(\eta - \beta\mathrm{k}_1), \quad (14)$$
$$\pi_3 = \mathrm{x}(\rho + \mu)(\eta - \beta\mathrm{k}_1)(1 - \Re_0),$$

with $x = \mu + \mu_0 + \omega$.

Applying the Routh–Hurwitz stability criteria, the equilibrium E_0 is locally asymptotically stable if all coefficients $\pi_1 > 0$, $\pi_2 > 0$, $\pi_3 > 0$, and $\pi_1\pi_2 > \pi_3$. Note that under the condition $\mathcal{R}_0 < 1$, it follows that $\eta - \beta k_1 > 0$, which ensures that $\pi_3 > 0$. Consequently, all Routh–Hurwitz conditions are satisfied. Therefore, all eigenvalues have negative real parts, and we conclude that the DFE E_0 is locally asymptotically stable if $\mathcal{R}_0 < 1$.

Theorem 2. *The DFE E_0 of the represented by (1) is globally asymptotically stable in the feasible region Ω whenever the basic reproduction number satisfies $\mathcal{R}_0 \leq 1$.*

Proof. To establish the global stability of the DFE, we construct a suitable Lyapunov function defined as

$$L = K_1E + K_2A + K_3I,$$

where K_1, K_2, and K_3 are positive constants to be determined. Taking the time derivative of L along the trajectories of the system (1), we obtain

$$L' = K_1E' + K_2A' + K_3I'. \quad (17)$$

Using the differential equations from system (1), we substitute the derivatives

$$L' = K_1\left[\frac{\beta S}{N}(I + k_1E + k_2A) - (\mu + \gamma + \sigma + \alpha)E\right]$$
$$+K_2[\alpha E - (\rho + \rho_1 + \mu)A] + K_3[\gamma E - (\mu + \mu_0 + \omega)I]. \quad (18)$$

Rearranging terms in (18) gives

$$L' = \left[K_1\frac{\beta S}{N} - K_3(\mu + \mu_0 + \omega)\right]I$$
$$+\left[K_1k_1\frac{\beta S}{N} - K_1(\mu + \gamma + \sigma + \alpha) + K_2\alpha + K_3\gamma\right]E$$
$$+\left[K_1k_2\frac{\beta S}{N} - K_2(\rho + \rho_1 + \mu)\right]A.$$

Since $S(t) \leq N(t)$ for all t, we have $\frac{S}{N} \leq 1$. Choose the constants as follows

$$K_1 = (\mu + \mu_0 + \omega)(\rho + \rho_1 + \mu), \quad K_2 = k_1(\mu + \mu_0 + \omega), \quad K_3 = k_2(\rho + \rho_1 + \mu).$$

Substituting these into Eq. (19), we find that all coefficients become non-positive when $\mathcal{R}_0 \leq 1$, implying $L' \leq 0$, with equality only when $E = A = I = 0$.

By LaSalle's Invariance Principle, all trajectories approach the largest invariant set where $L' = 0$, which corresponds to the DFE E_0. Hence, E_0 is globally asymptotically stable in Ω when $\mathcal{R}_0 \leq 1$.

Theorem 3. *The solutions of the SEIAVR model remain non-negative for all $t \geq 0$, provided the initial conditions satisfy*

$$S(0) \geq 0, \quad E(0) \geq 0, \quad I(0) \geq 0, \quad A(0) \geq 0, \quad V(0) \geq 0, \quad R(0) \geq 0.$$

Then, the model ensures that

$$S(t) \geq 0, \quad E(t) \geq 0, \quad I(t) \geq 0, \quad A(t) \geq 0, \quad V(t) \geq 0, \quad R(t) \geq 0$$

for all $t \geq 0$.

Proof. We consider the SEIAVR model defined by the system of equations in (6):

$$\begin{cases} \frac{dS}{dt} = \Lambda - \beta\lambda_1S + \eta_vV + \theta R - (\phi_v + \mu)S, \\ \frac{dE}{dt} = \beta\lambda_1S - (\mu + \gamma + \epsilon_2 + \sigma + \alpha)E, \\ \frac{dI}{dt} = \gamma E - (\mu + \mu_0 + \omega)I, \\ \frac{dA}{dt} = \alpha E - (\rho + \rho_1 + \mu)A, \\ \frac{dV}{dt} = \phi_vS + \epsilon_2E + \rho_1A - (\mu + \eta_v)V, \\ \frac{dR}{dt} = \omega I + \sigma E + \rho A - (\mu + \theta)R. \end{cases} \quad (20)$$

We verify positivity by checking that if a compartment becomes zero, its derivative is non-negative

i. Positivity of $S(t)$: If $S = 0$, then $\frac{dS}{dt} = \Lambda + \eta_vV + \theta R \geq 0$

since $V, R \geq 0$. Thus, $S(t)$ cannot become negative.

ii. Positivity of $E(t)$: If $E = 0$, then $\frac{dE}{dt} = \beta\lambda_1S \geq 0$ as $S \geq 0$.

Hence, $E(t)$ remains non-negative. (19)

iii. Positivity of $I(t)$: If $I = 0$, then $\frac{dI}{dt} = \gamma E \geq 0$ since $E \geq 0$.

Thus, $I(t) \geq 0$.

iv. Positivity of $A(t)$: If $A = 0$, then $\frac{dA}{dt} = \alpha E \geq 0$ with $E \geq 0$.

So, $A(t) \geq 0$.

v. Positivity of $V(t)$: If $V = 0$, then $\frac{dV}{dt} = \phi_vS + \epsilon_2E + \rho_1A \geq 0$ since all terms are non-negative. Therefore, $V(t) \geq 0$.

vi. Positivity of $R(t)$: If $R = 0$, then $\frac{dR}{dt} = \omega I + \sigma E + \rho A \geq 0$.

Thus, for non-negative initial conditions and positive parameters, each compartment remains non-negative for all $t \geq 0$.

Theorem 4. *Consider the SEIAVR model defined by Eq. (6). The DFE is locally asymptotically stable if the control reproduction number* $\mathcal{R}_v^0 \leq 1$. *Furthermore, when* $\mathcal{R}_v^0 > 1$, *the model admits at least one endemic equilibrium point*

$$E^* = (S^*, E^*, I^*, A^*, V^*, R^*),$$

with all components strictly positive.

Proof. To analyze the endemic equilibrium, we set the right-hand sides of system (6) to zero. Let the total population at equilibrium be

$$N^* = S^* + E^* + I^* + A^* + V^* + R^*. \tag{21}$$

Define the force of infection at equilibrium as

$$\lambda^* = \beta \cdot \frac{I^* + k_1 E^* + k_2 A^*}{N^*}. \tag{22}$$

At steady state, the model equations become

$$0 = \Lambda - \lambda^* S^* + \eta_v V^* + \theta R^* - (\phi_v + \mu) S^*,$$

$$0 = \lambda^* S^* - (\mu + \gamma + \epsilon_2 + \sigma + \alpha) E^*, \tag{24}$$

$$0 = \gamma E^* - (\mu + \mu_0 + \omega) I^*, \tag{25}$$

$$0 = \alpha E^* - (\rho + \rho_1 + \mu) A^*, \tag{26}$$

$$0 = \phi_v S^* + \epsilon_2 E^* + \rho_1 A^* - (\mu + \eta_v) V^*, \tag{27}$$

$$0 = \omega I^* + \sigma E^* + \rho A^* - (\mu + \theta) R^*. \tag{28}$$

From equations (24), (25), and (26), we solve

$$\begin{cases} E^* &= \frac{\lambda^* S^*}{\mu+\gamma+\epsilon_2+\sigma+\alpha}, \\ I^* &= \frac{\gamma E^*}{\mu+\mu_0+\omega}, \\ A^* &= \frac{\alpha E^*}{\rho+\rho_1+\mu}. \end{cases} \tag{29}$$

Substituting equations (29) into the remaining equations yields a nonlinear equation in λ^*, typically of quadratic or cubic form

$$a_1(\lambda^*)^2 + a_2\lambda^* + a_3 = 0, \tag{30}$$

where the coefficients a_1, a_2, a_3 depend on model parameters. Notably,

$$a_3 \propto (1 - \mathcal{R}_v^0). \tag{31}$$

Thus, if $\mathcal{R}_v^0 < 1$, then $a_3 > 0$, implying no positive root λ^*, and the DFE is the only biologically feasible solution. If $\mathcal{R}_v^0 > 1$, then $a_3 < 0$, and a positive root $\lambda^* > 0$ exists, implying the presence of an endemic equilibrium E^* with all state variables positive. This confirms the role of $\mathcal{R}_v^0$ as a threshold parameter separating disease extinction from persistence.

Theorem 5. *Consider the SEIAVR model given by system of Eq. (6). The model admits a unique DFE*

$$E_v^0 = (S^0, E^0, I^0, A^0, V^0, R^0), \tag{32}$$

where $E^0 = I^0 = A^0 = 0$. If the vaccination reproduction number satisfies $\mathcal{R}_v^0 < 1$, then the DFE E_v^0 is globally asymptotically stable in the region Ω_v.

Proof. Define a Lyapunov function based on the infectious compartments

$$L(t) = q_1 E(t) + q_2 A(t) + q_3 I(t), \tag{33}$$

where $q_1, q_2, q_3 > 0$ are constants to be chosen. Differentiating $L(t)$ with respect to time and substituting from system (6), we get

$$\frac{dL}{dt} = q_1 \left[\beta \frac{I + k_1 E + k_2 A}{N} S - (\mu + \gamma + \epsilon_2 + \sigma + \alpha) E\right]$$

$$+q_2[\alpha E - (\rho + \rho_1 + \mu) A] + q_3[\gamma E - (\mu + \mu_0 + \omega) I]. \tag{34}$$

Choose

$$\begin{cases} q_1 &= (\rho + \rho_1 + \mu)(\mu + \mu_0 + \omega), \\ q_2 &= \beta(\mu + \mu_0 + \omega), \\ q_3 &= \beta(\rho + \rho_1 + \mu). \end{cases} \tag{35}$$

Substituting equations (35) into (34) and simplifying yields

$$\frac{dL}{dt} \leq C \cdot (\mathcal{R}_v^0 - 1) \cdot E(t), \tag{36}$$

where

$$C = (\mu + \gamma + \epsilon_2 + \sigma + \alpha)(\rho + \rho_1 + \mu)(\mu + \mu_0 + \omega) > 0. \tag{37}$$

Hence, if $\mathcal{R}_v^0 < 1$, then $\frac{dL}{dt} < 0$ whenever $E(t) > 0$.

Equality holds if and only if $E = A = I = 0$.

By LaSalle's Invariance Principle, all trajectories in the region Ω_1 approach the largest invariant set within $\{E = A = I = 0\}$, which corresponds to the DFE E_v^0. Thus, the DFE is globally asymptotically stable when $\mathcal{R}_v^0 < 1$.

To evaluate the reliability of the SEIAVR model, we compare the simulated infection trajectories with

reported COVID-19 case data. This validation step is essential to ensure that the model adequately captures the observed transmission dynamics. By confronting model predictions with empirical data, we assess whether the chosen parameter set particularly those related to vaccination produces realistic epidemic patterns. The agreement between simulated and reported trends increases confidence in the model's suitability for forecasting and policy assessment, while also revealing possible discrepancies that may require further refinement.

The vaccination parameter η_v represents the effective rate at which susceptible individuals acquire protection. Its value plays a central role in shaping the epidemic trajectory. We determine η_v through calibration against real infection data by examining alternative parameter values and selecting the one that best reproduces both the early exponential growth phase and the subsequent decline in reported cases. This calibration procedure not only improves the empirical consistency of the model but also highlights the sensitivity of infection dynamics to vaccination intensity.

Fig. 4 presents a comparison between reported infection data from the United Kingdom [27] and the corresponding fitted curves generated by the SEIAVR Eq. (6) under different values of η_v. The observed data are shown as blue markers, whereas the solid curve represents the model prediction. The simulations were carried out using Python,

providing a direct quantitative link between observed epidemiological patterns and model-based analysis.

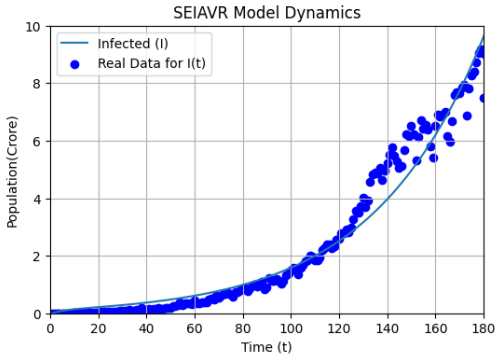

(a) For $\eta_v = 0.3410$

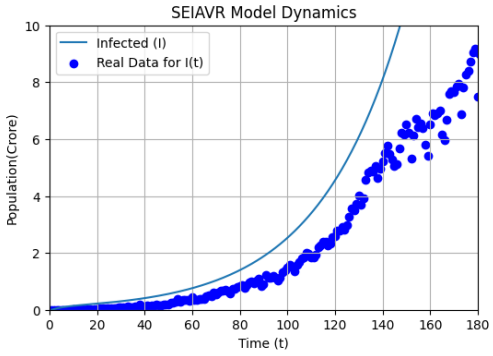

(b) For $\eta_v = 0.0698$

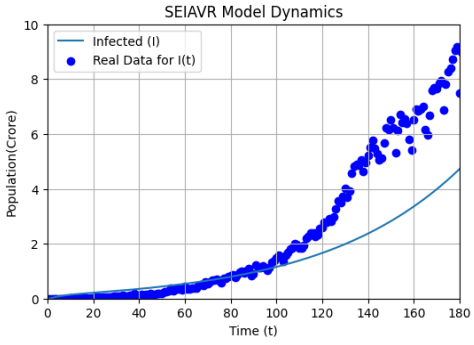

For $\eta_v = 0.1240$

Figure 4: Curve fitting with real and fitted data of Infection for different values of η_v.

Beyond numerical fitting, a rigorous analytical investigation of the SEIAVR framework is required to understand its qualitative behavior. The derivation of equilibrium points, computation of the basic reproduction number, and stability analysis yield threshold conditions that determine whether the infection persists or dies out. These theoretical results are independent of particular simulation scenarios and therefore provide general insight into the structural properties of the model.

At the same time, analytical techniques alone cannot fully capture the transient dynamics generated by time-dependent vaccination rates and Bang–Bang control interventions. Owing to the nonlinear nature of the system, closed-form solutions are generally unattainable. Numerical simulations therefore play a complementary role by illustrating time evolution, exploring the impact of varying control intensities, and supporting validation against real-world data.

The integration of analytical and numerical approaches thus strengthens both the mathematical foundation and the practical applicability of the model. Analytical results ensure theoretical consistency, while simulations demonstrate its relevance for epidemic management and intervention planning.

To investigate effective strategies for minimizing COVID-19 transmission, we apply optimal control theory to the model defined by Eq. (6). Our aim is to reduce the infection rate and limit the spread of the virus within the community through the implementation of four time-dependent control variables. These control strategies are defined as follows $u_1(t)$ represents isolation measures aimed at reducing contact between susceptible and infectious individuals, including hand hygiene, mask usage, avoidance of crowded areas, and travel restrictions. $u_2(t)$ denotes social awareness interventions, such as rapid diagnostic testing, contact tracing, and public health campaigns to promote early detection and isolation of exposed or infected individuals. Finally, $u_3(t)$ corresponds to treatment strategies for diagnosed COVID-19 cases, covering both symptomatic and asymptomatic patients, managed in healthcare facilities or under supervised quarantine to mitigate disease progression and transmission.

These control strategies form the foundation for the subsequent formulation of an optimal control problem based on the modified epidemiological model.

4. Optimal Control Problem Formulation

$$\begin{cases} \frac{dS(t)}{dt} = \Lambda - \beta(I + k_1E(t) + k_2A(t))\frac{S(t)}{N(t)}(1-u_1(t)) + \eta_v V - (\phi_v + \mu)S(t), \\ \frac{dE(t)}{dt} = \beta(I + k_1E(t) + k_2A(t))\frac{S(t)}{N(t)}(1-u_1(t)) \\ -(\mu + (1-u_2(t))\gamma + \epsilon_2 + \sigma + \alpha)E(t), \\ \frac{dI(t)}{dt} = \gamma(1-u_2(t))E(t) - (\mu + \mu_0 + (1+u_3(t))\omega)I(t), \\ \frac{dA(t)}{dt} = \alpha E(t) - (\rho + \rho_1 + \mu)A(t), \\ \frac{dV(t)}{dt} = \phi_v S(t) + \epsilon_2(t)E + \rho_1 A(t) - (\mu + \eta_v)V(t), \\ \frac{dR(t)}{dt} = \omega(1+u_3(t))I(t) + \sigma E(t) + \rho A(t) - \mu R(t). \end{cases} \tag{38}$$

The state variables are constrained to be non-negative, with non-negative initial conditions. The primary objective is to minimize the following function

$$J(u_1,u_2,u_3) = \int_0^{T_f} (C_1E(t) + C_2V(t) + C_3I(t) + \frac{1}{2}(C_4u_1^2(t) + C_5u_2^2(t) + C_6u_3^2(t)))\,dt,$$

subject to the control system described In Eq. (38).

The constants C_j for $j = 1,2,\dots,6$ are the weighting factors, while T_f represents the final time. Since the cost of intervention is nonlinear, quadratic control terms are employed, reflecting that the relationship between intervention cost and its effect on infected individuals is not linear. The controls introduced are Lebesgue integrable and bounded functions. Our objective is to determine the optimal controls u_i^* for $i = 1,\dots,3$, such that

$$J(u_i^*) = \min_U J(u_i). \tag{40}$$

where U represents the set of acceptable control functions, defined as

$$U = \{u_i[0,T_f] \to [0,1] \mid u_i \text{isLebesguemeasurable}\}.$$

4.1 Characteristics of optimal controls

The necessary conditions that must be met for any optimal control can be derived using Pontryagin's maximum principle. This principle provides a framework for transforming the optimal control problem into a system of differential equations containing state variables, adjoint variables, and optimality conditions for the control function [28]. This principle reformulates the system of equations (38) and (39) into a problem of minimizing the Hamiltonian point-wise with respect to the controls. The Hamiltonian Eq. (41) is expressed as follows

$$\begin{aligned} H \quad &= (C_1E + C_2V + C_3I) + \tfrac{1}{2}(C_4u_1(t)^2 + C_5u_2(t)^2 + C_6u_3(t)^2) \\ &+\lambda_1\left[\Lambda - \beta(I + k_1E + k_2A)\tfrac{S}{N}(1-u_1) + \eta_vV + \theta R - (\phi_v + \mu)S\right] \\ &+\lambda_2\left[\beta(I + k_1E + k_2A)\tfrac{S}{N}(1-u_1) - (\mu + (1-u_2)\gamma + \epsilon_2 + \alpha + \sigma)E\right] \\ &+\lambda_3[\gamma(1-u_2)E - (\mu + \mu_0 + (1+u_3)\omega)I]\lambda_4[\alpha E - (\rho + \rho_1 + \mu)A] \\ &+\lambda_5[\phi_vS + \epsilon_2E + \rho_1A - (\mu + \eta_v)V] \\ &+\lambda_6[\omega(1+u_3)I + \sigma E + \rho A - (\mu + \theta)R], \end{aligned} \tag{41}$$

where the symbols λ_m, for $m = 1,2,\dots,6$, represent the associated costate variables $S(t), E(t), I(t), A(t), V(t)$ and $R(t)$. The costate equations are given by

$$\begin{cases} \frac{d\lambda_1}{dt} = \frac{\partial H}{\partial S} = -\lambda_1\left[\frac{\beta(I+k_1E+k_2A)(1-u_1(t))}{N} - (\phi_v + \mu)\right] \\ \quad +\lambda_2\left[\frac{\beta(I+k_1E+k_2A)(1-u_1(t))}{N}\right] + \lambda_5\phi_v, \\ \frac{d\lambda_2}{dt} = \frac{\partial H}{\partial E} = C_1 - \lambda_1\frac{\beta k_1(1-u_1(t))}{N} \\ \quad +\lambda_2\left[\frac{\beta k_1(1-u_1(t))}{N} - (\mu + \gamma(1-u_2(t)) + \epsilon_2 + \sigma + \alpha)\right] \\ \quad +\lambda_3\gamma(1-u_2(t)) + \lambda_4\alpha + \lambda_5\epsilon_2 + \lambda_6\sigma, \\ \frac{d\lambda_3}{dt} = \frac{\partial H}{\partial I} = C_3 - \lambda_1\frac{\beta S(1-u_1(t))}{N} \\ \quad +\lambda_2\frac{\beta S(1-u_1(t))}{N} - \lambda_3(\mu + \mu_0 + (1+u_3(t))\omega) + \lambda_6\omega(1+u_3(t)), \\ \frac{d\lambda_4}{dt} = \frac{\partial H}{\partial A} = -\lambda_1\left[\frac{\beta k_2S(1-u_1(t))}{N}\right] \\ \quad +\lambda_2\left[\frac{\beta k_2S(1-u_1(t))}{N}\right] - \lambda_4(\mu + \rho + \rho_1) + \lambda_5\rho_1 + \lambda_6\rho, \\ \frac{d\lambda_5}{dt} = \frac{\partial H}{\partial V} = C_2 + \lambda_1\eta_v - \lambda_5(\mu + \eta_v), \\ \frac{d\lambda_6}{dt} = \frac{\partial H}{\partial R} = \lambda_1\theta - \lambda_6(\mu + \theta). \end{cases} \tag{42}$$

The following conditions give the optimal controls

$$\begin{cases} \frac{\partial H}{\partial u_1(t)} = C_4 u_1(t) + \lambda_1 \frac{\beta(I+k_1E+k_2A)S}{N} - \lambda_2 \frac{\beta(I+k_1E+k_2A)S}{N} = 0, \\ u_1(t) = \frac{(\lambda_2-\lambda_1)\beta(I+k_1E+k_2A)S}{NC_4}, \\ \frac{\partial H}{\partial u_2(t)} = C_5 u_2(t) + \lambda_2\gamma E - \lambda_3\gamma E = 0, \\ u_2(t) = \frac{(\lambda_3-\lambda_2)\gamma E}{C_5}, \\ \frac{\partial H}{\partial u_3(t)} = C_6 u_3(t) - \lambda_3\omega I + \lambda_6\omega I = 0, \\ u_3(t) = \frac{(\lambda_6-\lambda_3)\omega I}{C_6}. \end{cases} \tag{43}$$

Now we would like to examine the impact of various control strategies. The following Fig. 5 shows the results of these interventions and their effect on infection dynamics.

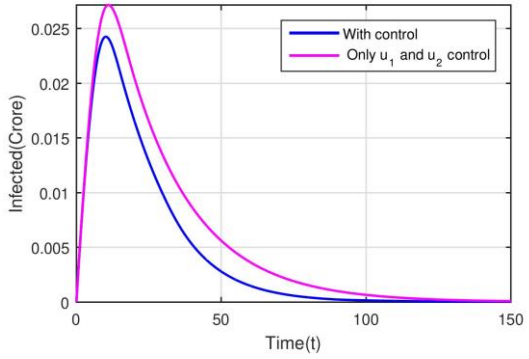

(a) Infected with and (u_1 and u_2)

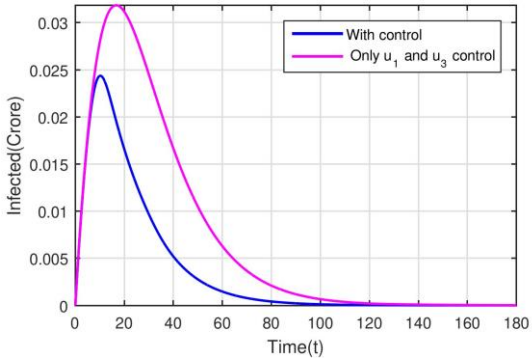

(b) Infected with and (u_1 and u_3)

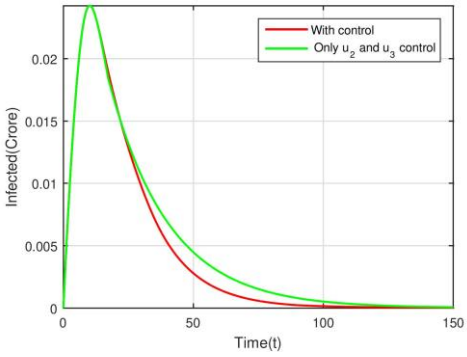

(c) Infected with and (u_2 and u_3)

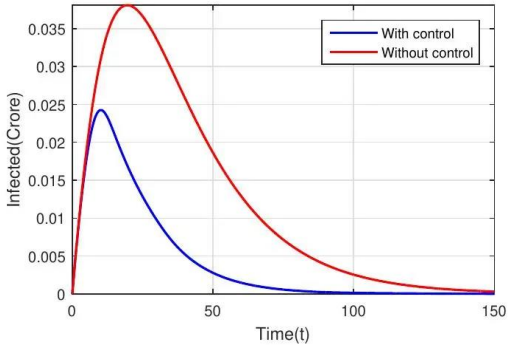

(d) Infected with and without controls

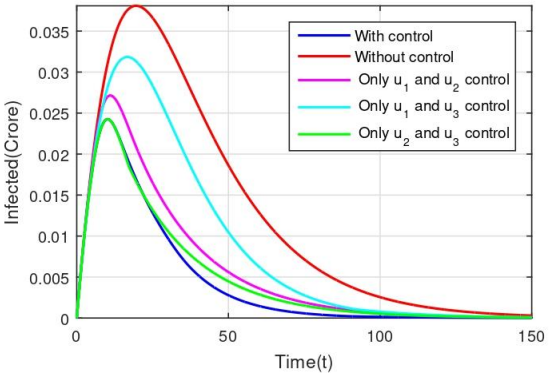

(e) Infected with all controls

Figure 5: Comparison of infected individuals under various control scenarios, including isolation (u_1), social awareness (u_2), and treatment (u_3), as well as without control.

To investigate the impact of key epidemiological parameters on infection dynamics, we consider variations in the recovery rate ω and the progression rate γ. The model is simulated under different parameter values while keeping other parameters fixed as in Table 1. The corresponding infection population trajectories are illustrated below in Fig. 6.

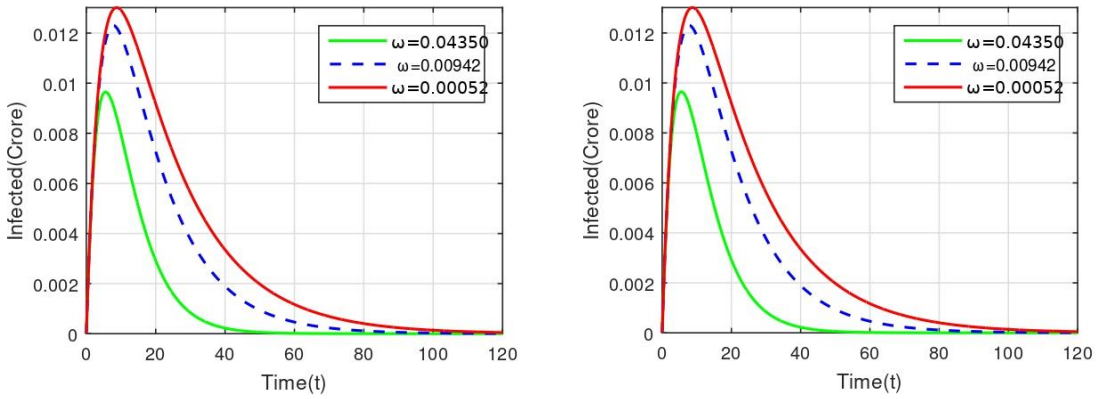

a) The Infection situation of three ω (b) The infection situation of three γ

Figure 6: Infection population scenarios under different parameter settings.

To explore the influence of vaccination-related parameters on population dynamics, we analyze variations in the vaccination rate ϕ_v, the waning rate of vaccine-induced immunity η_v, the transition rate from asymptomatic to vaccinated individuals ρ_1, and the progression rate from exposed to vaccinated individuals ϵ_2. The resulting vaccination trajectories are illustrated below in Fig. 7 under different parameter settings, while other parameters remain fixed as in Table 1.

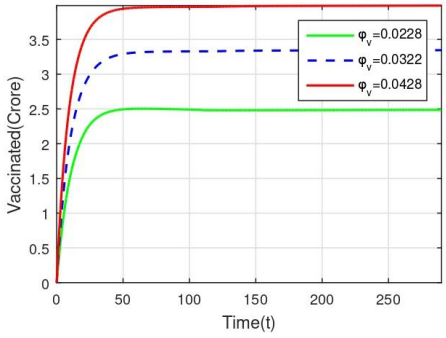

(a) Vaccinated for three values of ϕ_v

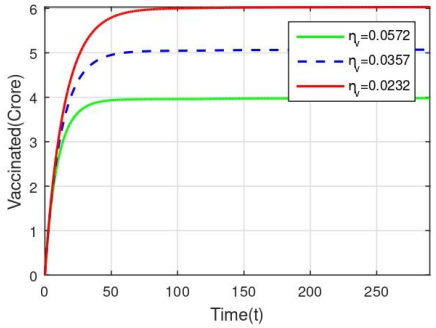

(b) Vaccinated for three values of μ_v

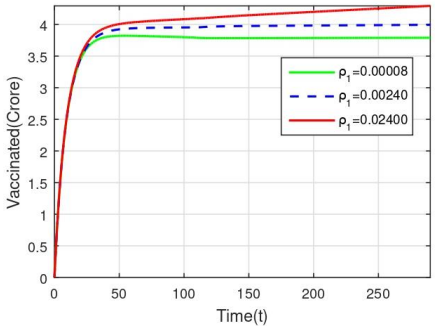

(c) Vaccinated for three values of ρ_1

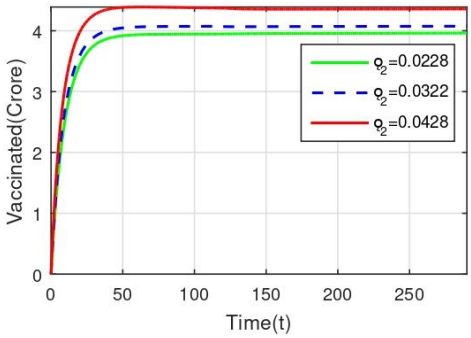

(d) Vaccinated for three values of ϵ_2

Figure 7: Scenario of Vaccination for different parameters.

To investigate the recovery dynamics of the population, we consider the impact of different parameter variations on the recovered class. Specifically, we examine the influence of the transition parameter ω, the treatment-related parameter ρ, and the recovery rate parameter σ. The recovery curves corresponding to these parameter settings are presented in Fig. 8, while the remaining parameters are kept fixed as listed in Table 1.

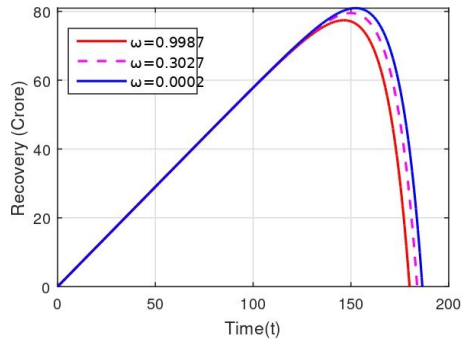

(a) Recovery for ω

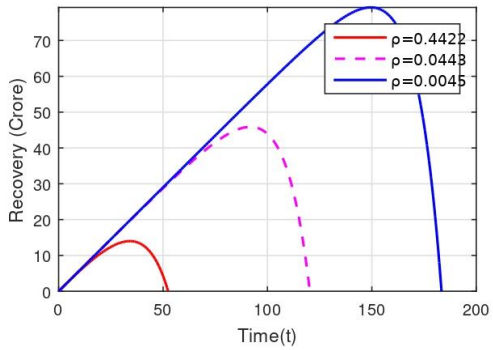

(b) Recovery for ρ

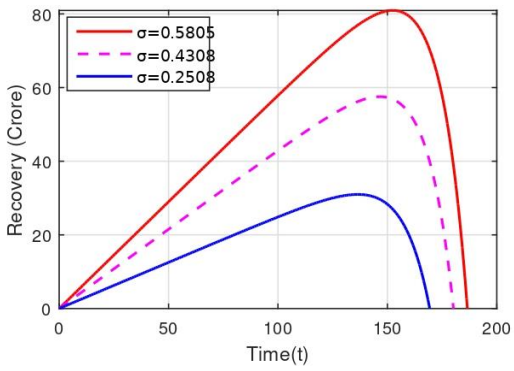

(c) Recovery for σ

Figure 8: Curve fitting with real and fitted data of Infection for different values of η_v.

5. SEIAVR Model with Bang-Bang Control and Cost-Effectiveness Analysis

5.1 Bang-Bang Control

To enhance both the predictive capability and practical applicability of the SEIAVR framework, we incorporate an optimal control formulation into the model. In this study, particular attention is given to a Bang–Bang control strategy, characterized by interventions that switch between extreme values rather than evolving continuously over time. This type of control structure reflects the way public health policies are often implemented in practice. Authorities typically enforce strict measures during periods of rapid transmission and subsequently relax them once infection levels decline. By adopting this on–off intervention mechanism, the model more realistically represents abrupt policy adjustments observed during epidemic outbreaks.

Let $\Gamma(t)$ denote the bang–bang control variable. This parameter models temporary closure policies or abrupt behavioral changes in response to rising infections. The control variable $\Gamma(t)$ takes binary values, where $\Gamma(t) = 1$ indicates the activation of strict intervention (such as closure or maximum reduction of contact), and $\Gamma(t) = 0$ corresponds to the absence of such measures. By integrating $\Gamma(t)$ into the system, alongside the existing continuous controls $u_1(t)$, $u_2(t)$, and $u_3(t)$, the model reflects both gradual behavioral modifications and immediate large-scale interventions. This combined framework establishes the foundation for the controlled SEIAVR model defined by Eq. (38) described below.

$$
\begin{cases}
\frac{dS}{dt} = \Lambda - \beta(I + k_1E + k_2A)\frac{S}{N} \underbrace{(1-u_1(t))(1-\kappa\,\Gamma(t))}_{\text{behavioralcontrol}\times\text{bang}--\text{bangclosure}} + \eta_v V \\
\quad -(\phi_v + \mu)S, \\
\frac{dE}{dt} = \beta(I + k_1E + k_2A)\frac{S}{N}\,(1-u_1(t))(1-\kappa\,\Gamma(t)) - [\mu + (1-u_2(t))\gamma \\
\quad +\epsilon_2 + \sigma + \alpha]E, \\
\frac{dI}{dt} = \gamma(1-u_2(t))E - [\mu + \mu_0 + (1+u_3(t))\omega]I, \\
\frac{dA}{dt} = \alpha E - (\rho + \rho_1 + \mu)A, \\
\frac{dV}{dt} = \phi_v S + \epsilon_2 E + \rho_1 A - (\mu + \eta_v)V, \\
\frac{dR}{dt} = \omega(1+u_3(t))I + \sigma E + \rho A - \mu R.
\end{cases}
\tag{44}
$$

The primary objective of using Bang-Bang contrl is to reduce the spread of infection while accounting for the economic and social costs of implementing interventions over the finite time horizon $[0, T_f]$. In Eq. (44) we introduced four time-dependent control variables: $u_1(t)$, $u_2(t)$, $u_3(t)$ and $\Gamma(t)$, where $\Gamma(t)$ bang–bang closure. These controls act on different components of the model and represent strategies to limit disease transmission and mitigate its impact on the population.

$$J_\Gamma(u_1, u_2, u_3, \Gamma) = \int_0^{T_f} (C_1 E(t) + C_2 V(t) + C_3 I(t) + C_7 S(t) + \frac{1}{2}(C_4 u_1^2(t) + C_5 u_2^2(t) + C_6 u_3^2(t) + C_8 \Gamma^2(t))) \, dt. \quad (45)$$

$$\Gamma^*(t) = \begin{cases} 1, & \beta\kappa \frac{S(t)}{N(t)} X(t)(1 - u_1(t))(\lambda_S(t) - \lambda_E(t)) < -\frac{1}{2} C_8, \\ 0, & \beta\kappa \frac{S(t)}{N(t)} X(t)(1 - u_1(t))(\lambda_S(t) - \lambda_E(t)) > -\frac{1}{2} C_8, \\ \text{singular(either)}, & \text{ifequalityholds.} \end{cases}$$

The global outbreak of COVID-19 prompted rapid adaptation and development of pharmacological treatments. While some antiviral and anti-inflammatory agents were specifically formulated in response to SARS-CoV-2, others were repurposed from pre-existing treatments originally intended for different viral infections or autoimmune conditions. Table 1 summarizes the invention or initial discovery dates of major drugs utilized for treating COVID-19, along with their original medical applications and the year they were introduced into COVID-19 treatment protocols.

To evaluate the effectiveness of intervention strategies, firstly, we consider three continuous control variables $u_1(t)$,$u_2(t)$ and $u_3(t)$. In addition, $\Gamma(t)$ is introduced as a Bang-Bang(B-B) control, which alternates between its minimum and maximum levels to model abrupt policy interventions or resource-driven actions. We compare two scenarios: (i) applying only the continuous controls u_1, u_2 and u_3 and (ii) applying all controls, including the Bang-Bang control $\Gamma(t)$. This comparison highlights the added benefit of $\Gamma(t)$ in further lowering the infection peak and shortening the epidemic duration is shown in Fig. 9.

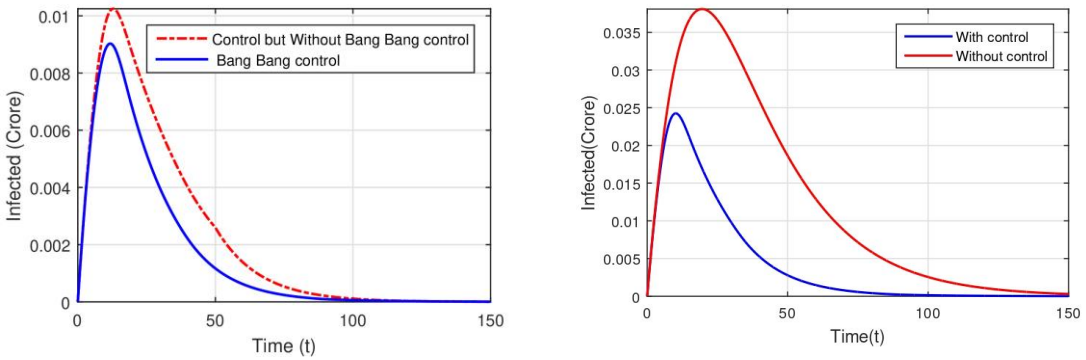

(a) Infected with B-B control (b) Infected without B-B control

Figure 9: Comparison of infected population under different control strategies (a) with Bang-Bang (B-B) control and (b) without Bang-Bang(B-B) control.

In Fig. 9(a), the blue solid curve (Bang-Bang control) shows a lower infection peak of approximately 0.009 crore cases, compared to the red dashed curve (only continuous controls), which peaks slightly higher at about 0.010 crore cases. Moreover, the decline in infections is faster under Bang-Bang control, reaching near zero by around $t = 80$–90 days, whereas without B-B control, infections persist until about $t = 100$ days. This indicates that Bang-Bang control accelerates recovery and reduces the overall epidemic burden. In Fig. 9(b), the comparison is between continuous control (blue) and no control (red). Without any control, the peak infection reaches nearly 0.037 crore cases, which is substantially higher than the peak under continuous control 0.024 crore cases. Additionally, the duration of infection is much longer in the absence of control, persisting until nearly $t = 120$–130 days, while under continuous control the epidemic subsides faster.

The inclusion of Bang-Bang (B-B) control clearly demonstrates its effectiveness in epidemic management. While continuous controls $u_1(t), u_2(t), u_3(t)$ already reduce the infection level compared to the no-control case, the additional application of $\Gamma(t)$ (B-B control) achieves two crucial outcomes:

• It further suppresses the infection peak, thereby reducing the maximum strain on healthcare resources.

• It accelerates the decline of infections, shortening the overall epidemic duration.

Hence, Bang-Bang control acts as a decisive intervention strategy, complementing continuous controls by ensuring both a lower epidemic burden and a faster return to normalcy.

5.2 Cost-Effective Analysis

To evaluate the economic viability of different COVID-19 intervention strategies, we conducted a cost-effectiveness analysis based on the total number of infections prevented, implementation costs, and two standard economic metrics: the Average Cost-Effectiveness Ratio (ACER) and the Incremental Cost-Effectiveness Ratio (ICER). We considered three strategies:

• **S1:** u_1, u_2, u_3 controls

• **S2:** u_1, u_2, u_3 + Vaccination

•**S3:** u_1, u_2, u_3 + Vaccination + Bang–bang control

To assess the economic performance of the proposed intervention strategies, we compute both the total implementation costs and the cumulative number of infections averted over the study horizon. Cost estimates and epidemiological reference values are obtained from published reports in England [29], which provide consistent data on healthcare expenditures and COVID-19 outcomes. This framework enables a structured comparison of the three strategies prior to presenting the quantitative results in Table 10.

Table 3: Cost-effectiveness comparison of intervention strategies.

Strategy	**Infections Averted**	**Total Cost**	**ICER**	**ACER**
S1	1.274×10^6	1.00×10^{11}	-0.006257	0.918302
S2	2.50×10^7	1.40×10^{12}	0.197754	0.197754
S3	5.594×10^6	1.10×10^{11}	-0.003117	0.061833

Table 3 shows that Strategy S2, which combines vaccination with large-scale standard control measures, achieves the highest number of infections averted. However, this improvement is accompanied by substantially higher total cost. Although its ICER and ACER values indicate that it remains economically justifiable, the magnitude of expenditure is considerably greater than that of the other strategies.

Strategy S3, which integrates vaccination with a Bang–Bang control mechanism, produces a notable reduction in infections while maintaining a

comparatively moderate total cost. Its lower ACER value suggests improved cost-efficiency relative to both S1 and S2. In contrast, Strategy S1 averts fewer infections and exhibits weaker economic performance under the adopted indicators.

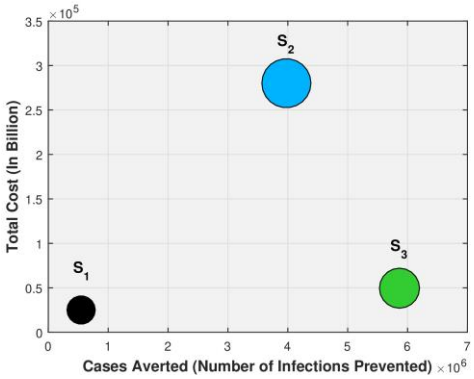

Figure 10: Bubble chart illustrating the trade-off between total cost and infections averted for each intervention strategy. Larger bubbles correspond to higher numbers of cases prevented.

The trade-off between expenditure and epidemiological benefit is further illustrated in Figure 4. The relative positioning of the strategies highlights the balance between resource allocation and health outcomes. In particular, the Bang–Bang-based strategy (S3) achieves a favorable compromise between effectiveness and cost.

The economic advantage of the Bang–Bang approach arises from its adaptive structure. Rather than maintaining continuous intervention intensity, the control switches between full implementation and relaxation according to epidemic conditions. Such a mechanism limits unnecessary expenditure during low-risk periods while retaining strong suppression capacity during high-transmission phases. As a result, infection peaks are reduced without sustaining prolonged high-cost measures.

From a resource-allocation perspective, adaptive on–off intervention policies may be especially relevant in settings with budget constraints. The results suggest that coupling vaccination with a targeted Bang–Bang control strategy can achieve meaningful reductions in infection burden while maintaining fiscal sustainability. This finding supports the inclusion of adaptive control mechanisms in epidemic policy design and economic planning.

6. Numerical Analysis

In Fig. 4(a), when $\eta_v = 0.3410$, the simulated infections rise sharply and exceed the observed data after approximately 100 days. This indicates that such a high vaccination-related parameter value does not adequately reflect the real transmission pattern. In Fig. 4(b), for $\eta_v = 0.0698$, the predicted trajectory increases more gradually and remains closer to the reported data over a longer period, although it underestimates infections during the later phase. Among the tested values, Fig. 4(c) with $\eta_v = 0.1240$ provides the best agreement, capturing both the early growth phase and the subsequent acceleration of infections. These comparisons demonstrate the strong sensitivity of the model to η_v and emphasize the necessity of careful parameter calibration to ensure reliable predictions.

Fig. 5 illustrates the time evolution of the infected population under different optimal control strategies. In Fig. 5(a), the combined use of isolation u_1 and social awareness u_2 substantially lowers the infection peak and shortens the outbreak duration compared to the uncontrolled scenario. Fig. 5(b) shows the joint implementation of isolation u_1 and treatment u_3, where infections decline more rapidly, reflecting the added effect of medical intervention. In Fig. 5(c), the combination of social awareness u_2 and treatment u_3 also produces a noticeable reduction in both peak magnitude and persistence. Fig. 5(d) compares the uncontrolled case with the scenario where all controls are applied, clearly indicating that the absence of intervention leads to a higher and more prolonged infection burden. Finally, Fig. 5(e) summarizes all strategies and shows that the simultaneous application of isolation, social awareness, and treatment (u_1, u_2, and u_3) yields the greatest reduction in infections.

A detailed comparison between partial and full intervention strategies further clarifies their relative performance. Although the combination of u_1 and u_2 in Fig. 5(a) reduces infections considerably, the peak remains higher than in the full-control scenario. The pair u_1 and u_3 in Fig. 5(b) achieves a faster decline than u_1 and u_2 but still does not match the suppression obtained when all controls are active. Similarly, u_2 and u_3 in Fig. 5(c) perform

effectively in the early stage yet are less efficient over longer periods. In contrast, Fig. 5(e) confirms that coordinating all three interventions produces the lowest peak and the fastest reduction in cases. This outcome aligns with the theoretical objective of the optimal control formulation, which seeks to minimize infections while accounting for intervention costs.

Fig. 6 examines the influence of the recovery rate ω and the progression rate γ on infection dynamics. In Fig. 6(a), increasing ω from 0.00052 (red) to 0.00942 (blue) and then to 0.04350 (green) progressively reduces the epidemic peak and accelerates its decline. The peak decreases from approximately 1.3×10^{-2} crore at $\omega = 0.00052$ (peak time ≈ 15 days) to about 1.15×10^{-2} crore at $\omega = 0.00942$ (peak ≈ 14 days), and further to nearly 9.5×10^{-3} crore at $\omega = 0.04350$ (peak ≈ 12 days). In addition, infections approach zero around 40 days for $\omega = 0.04350$, whereas they persist beyond 80 days when $\omega = 0.00052$. These results indicate that higher recovery rates significantly reduce both the magnitude and duration of the outbreak.

In Fig. 6(b), increasing γ from $\gamma_2 = 0.001822$ (blue) to $\gamma_1 = 0.004371$ (green) and further to $\gamma_3 = 0.008897$ (red) leads to a larger and earlier epidemic peak. The peak rises from approximately 1.0×10^{-2} crore at γ_2 (peak ≈ 15 days) to about 2.3×10^{-2} crore at γ_1 (peak ≈ 15 days), and reaches nearly 4.2×10^{-2} crore at γ_3 (peak ≈ 12 days). Thus, higher γ intensifies transmission, producing a sharper surge and prolonging elevated infection levels.

Overall, the two parameters influence the epidemic in opposite directions. Increasing ω mitigates transmission by lowering the peak and shortening the infectious period, whereas increasing γ amplifies and accelerates the outbreak. The variation in γ produces a larger change in peak magnitude compared with similar variation in ω, suggesting that the system is more sensitive to γ with respect to peak size. In contrast, ω exerts stronger influence on the tail behavior and time to elimination. These findings highlight the importance of interventions that reduce γ, such as contact reduction and rapid testing with isolation, together with measures that increase ω, including timely and effective treatment. Their combined implementation provides the most substantial suppression of infection. Fig. 7 illustrates the time evolution of the vaccinated population under parameter variations in the absence of control.

In Fig. 7(a), increasing ϕ_v from 0.0228 to 0.0322 and further to 0.0428 substantially elevates the vaccinated population. For $\phi_v = 0.0428$, saturation is reached most rapidly, approaching 4×10^7 individuals within the first 50 days, whereas smaller values lead to slower convergence. This confirms that larger ϕ_v accelerates vaccine uptake and increases overall coverage.

Fig. 7(b) demonstrates the effect of η_v. Raising η_v from 0.0232 to 0.0357 and then to 0.0572 significantly increases both the growth rate and final magnitude of vaccination. At $\eta_v = 0.0572$, the vaccinated population exceeds 5×10^7 individuals by approximately day 40, indicating that η_v strongly influences vaccination effectiveness.

In Fig. 7(c), variations in ρ_1 generate comparatively modest changes. Although increasing ρ_1 from 0.00008 to 0.02400 slightly accelerates early growth, the trajectories converge near 4×10^7 individuals. Thus, ρ_1 plays a secondary role relative to ϕ_v and η_v.

Fig. 7(d) presents the impact of ϵ_2. Larger values increase both the equilibrium coverage and the speed of convergence, with vaccination rising from below 3.8×10^7 to nearly 4.2×10^7 individuals as ϵ_2 increases. Overall, η_v exerts the strongest quantitative influence, followed by ϕ_v, whereas ρ_1 and ϵ_2 contribute more moderate adjustments to vaccination dynamics.

Fig. 8 displays recovery trajectories under different parameter values. Variations in ω primarily affect the timing and magnitude of recovery. When $\omega = 0.0002$, recovery progresses more slowly but ultimately reaches the highest peak (approximately 75 crore around day 150). Larger ω values produce earlier but lower peaks, indicating that increased recovery rates shorten the infectious period but reduce cumulative recovered totals.

The parameter ρ exhibits a limiting effect. At $\rho = 0.442$, recovery rises briefly but remains below 15 crore. Reducing ρ to 0.0448 improves outcomes, while $\rho = 0.0045$ yields the highest and most sustained recovery level (above 70 crore). This suggests that smaller ρ values support long-term

recovery persistence.

In contrast, σ shows a strong positive association with recovery magnitude. For $\sigma = 0.5805$, recovery exceeds 70 crore near day 150, whereas smaller σ values result in delayed and reduced peaks. Collectively, the sensitivity analysis indicates that smaller ρ, appropriately scaled ω, and larger σ values promote stronger and more sustained recovery dynamics.

Fig. 9 presents the infected population over a 150-day period under different intervention strategies. Fig. 9(a) compares Bang-Bang control with a continuous control strategy. Under Bang-Bang control, the infection peak is approximately 9×10^4 individuals around day 25, followed by a rapid decline to near elimination by day 90. The continuous strategy produces a slightly higher peak (about 1×10^5 individuals around days 30–32) and a slower reduction, with infections persisting beyond day 100.

Fig. 9(b) contrasts controlled and uncontrolled scenarios. Without intervention, infections peak at roughly 3.7×10^5 individuals around day 35 and persist until approximately day 140. The introduction of control measures substantially lowers both the peak magnitude and epidemic duration. These results confirm that Bang-Bang control achieves faster suppression and shorter outbreak duration compared with both continuous control and the uncontrolled case.

6.1 Advantages and Limitations of the Model and Methods

The proposed model offers several advantages, including a structured description of asymptomatic and symptomatic transmission, integration of vaccination and "stop-and-go" control strategies, and inclusion of cost-benefit analysis. Analytical techniques provide theoretical guarantees such as stability conditions and threshold behavior, while numerical simulations allow for evaluation and validation of real-world scenarios using empirical data.

However, the model also has limitations. It assumes a homogeneous population mix without considering spatial heterogeneity or population stratification. Furthermore, the "stop-and-go" approach simplifies intervention intensity to extreme levels and may not encompass all policy changes in the real world. Numerical simulations rely on the accuracy of parameter estimation, which can be affected by data quality.

7. Conclusion

This study developed and analyzed a vaccination-enhanced SEIAVR epidemic model to investigate the impact of vaccination and control strategies on the spread of COVID-19. We derived the optimal Bang-Bang control strategy using the Pontryagin maximum principle and validated the model using numerical simulations with real-world data from the UK. Combining vaccination with Bang-Bang control significantly reduced infection peak and shortened the duration of the epidemic. This integrated strategy achieved good cost-effectiveness and optimized the utilization of limited medical resources. The analysis confirmed the threshold conditions for the elimination of the disease under the proposed intervention. This model assumes a homogeneous population mix and simplifies certain aspects of the implementation of the intervention. Future research directions: More research could incorporate factors such as heterogeneous populations, age structure segmentation, random effects, and time delays, and assess the impact of policies under different medical and economic constraints. In general, this study highlights the importance of combining vaccination with dynamic control strategies to achieve effective epidemic management and support evidence-based public health policies.

References

[1] K. E. Jones, N. G. Patel, M. A. Levy, A. Storeygard, D. Balk, J. L. Gittleman, P. Daszak, Global trends in emerging infectious diseases, Nature 451 (7181) (2008) 990–993.

[2] C. Huang, Y. Wang, X. Li, L. Ren, J. Zhao, Y. Hu, L. Zhang, G. Fan, J. Xu, X. Gu, et al., Clinical features of patients infected with 2019 novel coronavirus in wuhan, china, The Lancet 395 (10223) (2020) 497–506.

[3] X. He, E. H. Y. Lau, P. Wu, X. Deng, J. Wang, X. Hao, Y. C. Lau, J. Y. Wong, Y. Guan, X. Tan, et al., Temporal dynamics in viral shedding and transmissibility of COVID-19, Nature Medicine 26 (5) (2020) 672–675.

[4] World Health Organization, Tracking sars-cov-2 variants (2021).

[5] D. M. Cutler, L. H. Summers, The costs of the COVID-19 pandemic, JAMA 324 (15) (2020) 1495–1496.

[6] N. M. Ferguson, D. Laydon, G. Nedjati-Gilani, et al., Impact of non-pharmaceutical interventions (npis) to reduce COVID-19 mortality and healthcare demand, Imperial College London (2020).

[7] World Bank, Global economic prospects (2021).

[8] S. Lenhart, J. T. Workman, Optimal Control Applied to Biological Models, Chapman and Hall/CRC, Boca Raton, FL, 2007.

[9] W. H. Fleming, R. W. Rishel, Deterministic and Stochastic Optimal Control, Springer, New York, 1975.

[10] K. O. Okosun, O. D. Makinde, Optimal control analysis of a malaria disease transmission model, Mathematical Biosciences 244 (2) (2013) 128–135.

[11] G. Giordano, F. Blanchini, R. Bruno, P. Colaneri, A. Di Filippo, A. Di Matteo, M. Colaneri, Modelling the COVID-19 epidemic and implementation of population-wide interventions in italy, Nature Medicine 26 (6) (2020) 855–860.38

[12] M. F. Drummond, M. J. Sculpher, K. Claxton, G. L. Stoddart, G. W.Torrance, Methods for the Economic Evaluation of Health Care Programmes, 4th Edition, Oxford University Press, Oxford, 2015.

[13] S. Ambani, T. Kuniya, Bang–bang control strategies in epidemic models with application to COVID-19, Mathematical Biosciences and Engineering 18 (6) (2021) 8453–8472.

[14] K. O. Okosun, O. D. Makinde, Optimal control analysis of a COVID-19 model with non-pharmaceutical interventions, Mathematical Biosciences 325 (2020) 108493.

[15] U. Felgenhauer, On stability of bang-bang type controls, SIAM Journal on Control and Optimization 41 (6) (2003) 1843–1867. doi:10.1137/ S0363012901399271.

[16] M. A. Kuddus, A. K. Paul, T. Theparod, Cost-effectiveness analysis of COVID-19 intervention policies using a mathematical model: an optimal control approach, Scientific Reports 14 (1) (2024) 494.

[17] B. Asamoah, et al., Global impact of covid-19 and modeling of intervention strategies, Journal of Infection and Public Health 13 (12) (2020)1805–1814.

[18] I. Peni, et al., Nonlinear modeling of COVID-19 dynamics with interventions, Nonlinear Dynamics 102 (2020) 1331–1348.

[19] A. Matouk, et al., Complex network-based seir modeling of COVID-19 transmission, Applied Mathematics and Computation 385 (2020)125459.

[20] W. Cullen, et al., Mental health implications and asymptomatic spread of COVID-19, International Journal of Environmental Research and Public Health 17 (11) (2020) 4019.

[21] H. Sun, et al., Modeling COVID-19 dynamics with asymptomatic carriers, Mathematical Biosciences and Engineering 17 (6) (2020) 4891–4911.

[22] O. J. Peter, H. S. Panigoro, A. Abidemi, M. M. Ojo, F. A. Oguntolu, Mathematical model of COVID-19 pandemic with double dose vaccination, Acta biotheoretica 71 (2) (2023) 9.39

[23] M. Gatto, E. Bertuzzo, L. Mari, S. Miccoli, L. Carraro, R. Casagrandi, A. Rinaldo, Spread and dynamics of the COVID-19 epidemic in italy:Effects of emergency containment measures, Proceedings of the National Academy of Sciences 117 (19) (2020) 10484–10491.

[24] M. A. Acuna-Zegarra, J. X. Velasco-Hernandez, A. Comas-Garcia, C. Castillo Garsow, A COVID-19 SEIR model with vaccination and waning immunity, Mathematical Biosciences 337 (2021) 108615.

[25] M. Razzaq, M. Shahzad, M. Arif, U. Ahmad, Optimal control strategies for COVID-19: Vaccination and treatment, Chaos, Solitons & Fractals 147(2021) 110912.

[26] A. Atangana, S. Araz, K. M. Owolabi, Modelling the dynamics of COVID-19 with fractional derivatives: Insights into control measures and vaccination, Results in Physics 19 (2020) 103425.

[27] UK Government, Coronavirus (COVID-19) in the uk, https:// coronavirus.data.gov.uk/, accessed: 2026-02-01 (2021).

[28] L. S. Pontryagin, Mathematical theory of optimal processes, Routledge, 2018.

[29] Public Health England, COVID-19 vaccine surveillance report published, GOV.UK news story, last updated 16 September 2021 (May 2021)